Biosensors and Bioelectronics 26 (2011) 3110–3114

Contents lists available at ScienceDirect

Biosensors and Bioelectronics

journal homepage: www.elsevier.com/locate/bios

Aptamer-based PDMS–gold nanoparticle composite as a platform for visual detection of biomolecules with silver enhancement

Wei Wang[a,b], Wen-Ya Wu[a], Xiaoqin Zhong[a], Wei Wang[a], Qiang Miao[a], Jun-Jie Zhu[a,*]

[a] Key Laboratory of Analytical Chemistry for Life Science (MOE), School of Chemistry and Chemical Engineering, Nanjing University, Nanjing 210093, PR China
[b] School of Chemical and Biological Engineering, Yancheng Institute of Technology, 9 Yingbin Road, Yancheng 224051, PR China

ARTICLE INFO

Article history:
Received 20 August 2010
Received in revised form 12 October 2010
Accepted 21 October 2010
Available online 28 October 2010

Keywords:
Aptamer
Visual detection
Silver enhancement
PDMS
Gold nanoparticles

ABSTRACT

A sensitive colorimetric detection for biomolecules based on aptamer was described. Poly(dimethylsiloxane) (PDMS)–gold nanoparticles (AuNPs) composite film was used as a platform for immobilizing anti-target aptamer. PDMS–AuNPs composite film only covered with aptamer showed high inhibiting ability towards silver reduction, after target molecules were conjugated on the modified surface, the catalytic efficiency of AuNPs for silver reduction was increased. In this system, the darkness density of silver enhancement was applied for target quantitative measurement. Lysozyme and adenosine 5′-triphosphate (ATP) were tested as the models, quantitative measurements with imaging software or semiquantitative measurements with naked eyes were carried out in the range of 1×10^{-2}–1 μg/mL and 1×10^{-4}–1×10^{3} μg/mL, the volume of reagent using in each assay is 15 μL or less. We speculated that aptamer-target conjugates' inhibition ability for AuNPs' catalytic efficiency toward silver reduction might come from charge and spatial effects. This study can offer a completely novel and relatively general approach for colorimetrical aptamer sensors with good analytical properties and potential applications. The sensor could be coupled with digital transmission of images for remote monitoring system in diagnosis, food control, and environmental analysis.

1. Introduction

Recently, one of the research interests in analytical chemistry is focused on producing low-cost, point-of-care diagnostics and environmental monitoring devices (Bercovici et al., 2010; Lutz et al., 2010; Ronen et al., 2009; Sia and Kricka, 2008; Yang et al., 2010). A number of rapid, simple, and inexpensive testing devices, such as paper-based indicators, dipstick test assays, and even paper chromatography, were introduced (Carvalhal et al., 2010; Liu et al., 2006; Yang and Wang, 2009). A remarkable publication in Whitesides' group described a method for quantifying multiple analytes using a patterned paper coupled with digital transmission of images to off-site diagnosticians (Martinez et al., 2008). And one of the most useful examples is the well-known commercially available pregnancy test kit.

Aptamers are single-stranded nucleic acids that can be selected from a large random library to bind a number of molecules with high affinity and specificity. Therefore, they are considered to be the nucleic acid version of antibodies (Wilson and Szostak, 1999; Jayasena, 1999). Since its first discovery in the early 1990s, the use of aptamers for sensing and diagnostic applications has been extensively explored. The key challenge to their applications is transforming the aptamer binding events into physically detectable signals. Because detection results can be observed with naked eyes without the need for sophisticated instruments, simple colorimetric sensors have been attracted much attention. Recent reports of colorimetric sensors based on aptamers are a positive step towards improving user-friendliness (Bai et al., 2010; Chen et al., 2008a; Huang et al., 2005; Liu and Lu, 2006; Wang et al., 2007; Zhang et al., 2009). Linear range of 4.4–132.7 μM for adenosine 5′-triphosphate (ATP) detection was found in free solution with colorimetric method (Wang et al., 2007). Many other approaches based on aptamer for biomolecules detection have also been reported. Fluorescence method was applied for adenosine in urine samples (Chen et al., 2008b) and for aptamer induced disassembly of fluorescent combined with magnetic nano-silica sandwich complex (Song et al., 2009). Aptamer-gold nanoparticles (AuNPs) conjugates was also a powerful sandwich element and an excellent amplification reagent for surface plasmon resonance-based sandwich immunoassay (Wang et al., 2009). And aptamer-modified AuNPs were used as selective probes and AuNPs as the surface-assisted laser desorption/ionization matrixes for the determination of ATP by mass spectrometry. (Huang and Chang, 2007).

Silver enhancement, a procedure for electroless silver deposition where the gold nanoparticles act as nuclei, has been widely used for immunoassays (Chen et al., 2007; Gupta et al., 2007;

* Corresponding author. Tel.: +86 25 83594976; fax: +86 25 83594976.
E-mail addresses: jjzhu@nju.edu.cn, jjzhu@netra.nju.edu.cn (J.-J. Zhu).

0956-5663/$ – see front matter © 2010 Elsevier B.V. All rights reserved.
doi:10.1016/j.bios.2010.10.034

Pan et al., 2008; Xu et al., 2009; Yeh et al., 2009; Zhang et al., 2009). High sensitivity could be obtained for the measurement. In this technique, colloidal metal particles act as catalysts to reduce silver ions to metallic silver, which is typically quantified by colorimetric and electrochemical measurement (Cai et al., 2002). A number of materials have already been applied as platform for colorimetry, such as silicon chip (Miao et al., 2009), glass surfaces (Nogami et al., 2009), gold electrodes (Cherevko and Chung, 2009). Poly(dimethylsiloxane) (PDMS) is one of the most widely used polymer materials for fabricating microfluidic chips due to its transparency, outstanding elasticity, good thermal and oxidative stability, ease to be fabricated and sealed with various materials. The surface of PDMS can be chemically modified or physically masked by adsorption to generate anionic, neutral, and cationic surface. A promising report is in-situ synthesis of PDMS–AuNPs composite films and its bioapplications (Zhang et al., 2008).

Besides the detections in free solution systems, substrate material which should be convenient fabrication is an important issue that should be absolutely considered among the component elements of colorimetric sensors. In this respect, we developed a single aptamer sensor based on PDMS–AuNPs composite film, and introduced silver enhancement on AuNPs surface covered with aptamer-target conjugations for colorimetric detection of biomolecules. Lysozyme is a ubiquitous protein in mammals and is often termed to as the "body's own antibiotic" and ATP is an important substrate in living organisms and have been used as indicators for cell viability and cell injury. Lysozyme and ATP were used as the models of proteins and small molecules in this research. Samples were treated with conventional phosphate buffered saline (PBS). Quantitative measurements with imaging software or semiquantitative measurements with naked eyes were carried out for lysozyme and ATP in the range of 1×10^{-2}–1 μg/mL and 1×10^{-4}–1×10^{3} μg/mL, respectively. We speculated that aptamer-target conjugates' inhibition ability for AuNPs' catalytic efficiency toward silver reduction might come from charge and spatial effects. This simple, rapid, and sensitive method does not require multiple operation steps such as ELISA on the surface, and the volume of reagent using in each well is 15 μL or less which is much less than usual electrochemical detections. Compared with the approaches mentioned above, this proposed method has the advantages of wide detection range, simple instrumentation, low production cost, and portability.

2. Materials and methods

2.1. Reagents and materials

The DNA oligonucleotides were purchased from Shanghai Shangon Biotechnology Corporation (Shanghai, China). All the oligonucleotides solutions were heat-treated in 90 °C for 3 min and then cooled in ice for 10 min prior to use. Anti-lysozyme aptamer has a sequence of 5′-HS-(CH_2)6-ATC TAC GAA TTC ATC AGG GCT AAA GAG TGC AGA GTT ACT TAG-3′, 42 nt. Anti-ATP aptamer has a sequence of 5′-HS-(CH_2)6-ACC TGG GGG AGT ATT GCG GAG GAA GGT-3′, 27 nt. 6-Mercapto-1-hexanol (MCH), lysozyme (from hen egg white) and Silver Enhancer Kit (SE-100) were products of Sigma–Aldrich (St.Louis, MO, USA). Adenosine 5′-triphosphate (ATP) was purchased from Nanjing Bookman Biotechnology Ltd. (Nanjing, China). $HAuCl_4 \cdot 4H_2O$ was from Shanghai Chemical Reagent Company (Shanghai, China). PDMS was obtained from Dow Corning (midland, MI, USA). Buffer solution for oligonucleotides contained 100 mM $Na_2HPO_4 + NaH_2PO_4$, 5 mM $MgCl_2$, pH 7.38. Image software Quantity One was purchased from BIO-RAD Company. UV–vis adsorption spectra were recorded on Perkin–Elmer Lamda 25 UV–vis spectrometer. All the other reagents were of analytical grade, and deionized water was used throughout.

2.2. Preparation of aptamer-based PDMS gold nanoparticle composite film

PDMS–AuNPs composite film was prepared as the described procedure in literatures (Wu et al., 2010; Zhang et al., 2008). Oligonucleotides were immobilized on the PDMS–AuNPs composite film after they were rinsed and dried with N_2, as shown in Fig. 1. A 15 μL aliquot of 2 μM pretreated aptamer solution (buffer solution, pH 7.38) was dropped into the wells. The chips were incubated at 4 °C in a moisture chamber overnight (12 h). After incubation, they were rinsed with rinsing buffer (50 mM PBS, pH 7.38, 0.05% Tween 20) to remove physically adsorbed aptamer. Then deionized water was used to rinse for three times. Finally the chip was dried with N_2. After the rinsing process, the chip was incubated with 1 mM MCH (10 mM PBS, pH 7.38) at 37 °C for 1 h and rinsed with rinsing buffer, deionized water, at last dried with N_2. Keep in store at 4 °C.

2.3. Colorimetric detection

After the blocking step, the aptamer-modified chip was incubated with 15 μL of detecting target samples for 1 h at 37 °C. After rinsing process, 15 μL silver enhancement solution (mixture of A and B solutions from the Silver Enhancer Kit in a 1:1 volume ratio prepared just prior to use) was dropped into each well, the chip was incubated in dark for 30 min, and at the same time we capture the live photos of the microarray using ordinary digital camera. In our experimental, camera and parameters are as follows: Olympus FE-210 digital camera with CCD sensor (Tokyo, Japan), maximum resolution 3072 × 2304 pixels, programmed auto exposure without flash light, the object distance is 30–40 cm.

These photos were imported into the computer and color differences were analysed by image software Quantity One (Bio-Rad company). Darkness density of each well was picked to describe color difference among the volume data in volume analysis report.

3. Results and discussion

3.1. Mechanism of gold nanoparticle-based silver enhanced aptamer sensor

The free AuNPs selected as highly useful colorimetric probes is because they cannot only catalyze silver reduction, but also can act as the nuclei for silver precipitation (Hacker, 1989). Yang et al. reported a label-free immunosensor which utilized the covering immunecomplex inhibiting ability to AuNPs catalytic efficiency toward silver reduction (Yang and Wang, 2009). With the similar principle, the PDMS–AuNPs composite film was also applied for immunoassay in our group (Wu et al., 2010). In this research, we developed a novel colorimetrical aptamer sensor on solid PDMS surface. Fig. 1 shows the procedure of the PDMS–AuNPs composite film based colorimetrical target aptamer sensor for both protein and small biomolecules (ATP) detection. It is interesting that the phenomenon is different from immunosensor mentioned above. With the formation of aptamer-target conjugates, the inhibiting ability to AuNPs catalytic efficiency toward silver reduction was decreased as shown in Fig. 2. Well A appears to be totally black because naked PDMS–AuNPs composite film with silver enhancement solution, so the catalytic reaction goes extremely fast while causing more silver deposition. Darkness density in well B is less than well A, because the aptamer molecules were immobilized on the AuNPs surface disorderly which inhibited the contact between AuNPs and silver enhancement solution. For well C, after MCH was

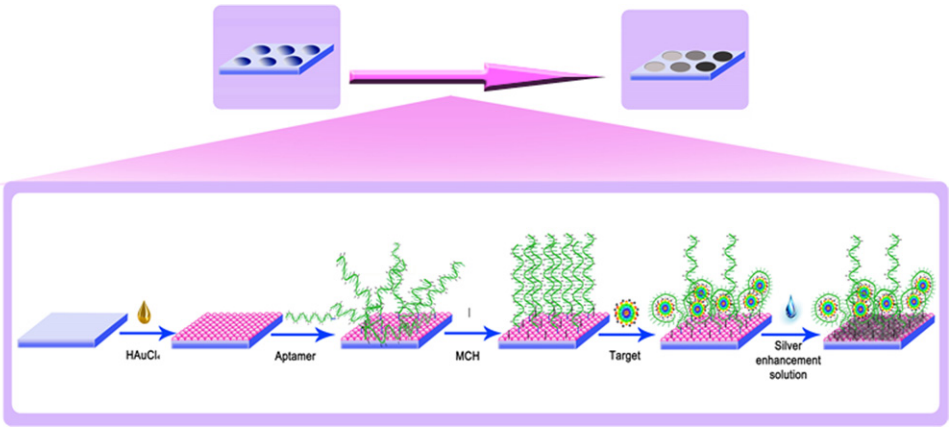

Fig. 1. Schematic illustration of preparation of PDMS–AuNPs based aptamer sensor and its application for biomolecules detection.

introduced to block other active sites on the surface, the darkness density became obviously lower than well B. This is because MCH can not only block the active sites, but also play a role of making aptamer sequences to become upright and orderly. The linear structure of aptamers has the strongest inhibiting ability toward silver reduction. As a result, well D is darker than well C because of the binding event in the presence of target.

We speculated the decrease of inhibition ability for aptamer-target conjugates were based on the two issues. Charge effect is one of them as shown in Fig. 3. The mechanism may be ascribed as the surface charge change (Cheng et al., 2007; Rodriguez et al., 2005). The electrostatic repulsion between the negatively-charged anti-target aptamer and silver lactate hinders the silver lactate being reduced by AuNPs where aptamer acts as an electrostatic barrier (lactate is an electron-rich molecule due to the presence of three oxygen atoms, and it acted as metal–ligand which combined with silver ion through coordination). The selective binding of the protein to the aptamer-functionalized PDMS surface results in diminishing of the surface charge that facilitates access of silver ions and its reaction on the PDMS–AuNPs film surface. Such unique recognition-induced diminishing of the surface charge leads to a highly sensitive silver enhancement signal. Second, it may be the reason of spatial effect as shown in Fig. 3. In the absence of target molecules, single aptamer sequences were immobilized onto the composite film surface disorderly. Together with MCH could make them straight up and become similar to a thick forest covering the AuNPs compactly, and the PDMS–AuNPs composite film only covered with aptamer and MCH bear high inhibiting ability towards silver reduction. The explanation is based on the literature (Liu and Lu, 2007). In order to confirm the phenomena, we compared the inhibiting ability of anti-target aptamer with two lengths, the results revealed that the inhibiting ability of 42-based aptamer stronger than that of 27-based one (shown in Fig. S1 in supplementary data). This thick barrier of aptamers could strongly inhibit the catalysis of AuNPs. When the target molecules were introduced, the aptamer switched its structure to bind targets and formed an aptamer-target wrapping package as various spatial configurations. As a result, structure of the compact barrier layer had been partially destroyed by bending events of some of the trees that aptamers bind to target molecules. Therefore, the destroyed barrier layer of aptamers resulted in a relatively weaker inhibiting ability.

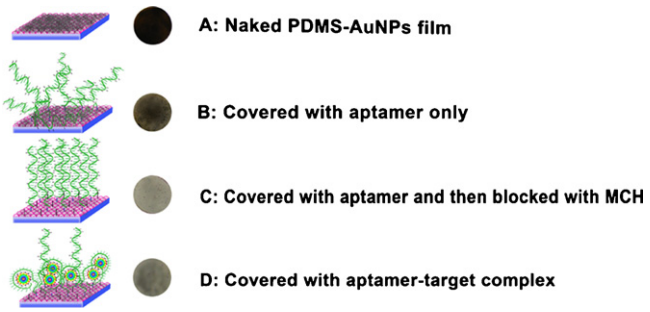

Fig. 2. The different status for inhibiting ability to AuNPs' catalytic efficiency toward silver reduction. Experimental conditions: PDMS–AuNPs composite film was fabricated according to the procedure in literatures (Wu et al., 2010); Aptamer covered chip was prepared with following procedure, A 15 μL aliquot of 2 μM pretreated aptamer solution was dropped into the wells and incubated overnight, then it was rinsed with buffer; Chip blocked with MCH, the chip was incubated with 1 mM MCH at 37 °C for 1 h and rinsed; Apatmer-target complex was followed by the procedure, the chip mentioned above was incubated with 15 μL of 10^{-1} μg/mL lysozyme for 1 h at 37 °C, then rinsed. 15 μL of silver enhancement solution was dropped into each well, the chip was incubated in dark for 30 min, and at the same time we capture the live photos of the microarray using ordinary digital camera.

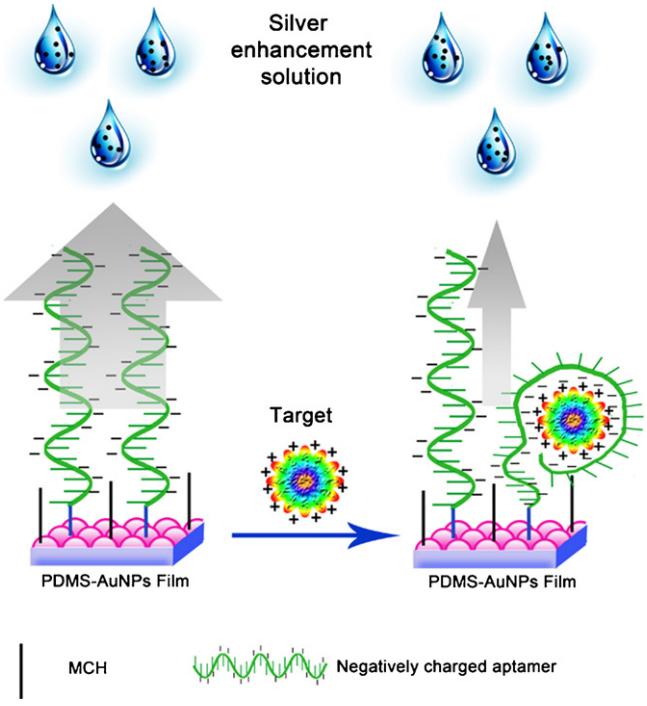

Fig. 3. Schematic illustration of charge effect and spatial effect. Decreasing of inhibition ability of aptamer-target conjugates facilitates access of silver ions on the PDMS–AuNPs film surface.

3.2. Characterization of aptamer immobilized on PDMS–AuNPs composite films

UV–vis absorption spectroscopy was used to monitor the absorption of aptamer which was immobilized onto the PDMS–AuNPs composite films. The absorption intensity between 254 nm and 275 nm increased after immobilization of aptamer onto the PDMS–AuNPs composite film, indicating the presence of aptamer which has a characteristic absorption peak around 260 nm. On the other hand, the absorption band centered at 530–534 nm results from the surface plasmon band of gold nanoparticles (Wang et al., 2006). The formation of aptamer-based PDMS–AuNPs was proved by a blue shift in the absorption peak from 530 nm (AuNPs) to 524 nm along with its increasing absorption intensity (shown in Fig. S2 in supplementary data).

Surface density of aptamers on the composite film was also investigated. Different surface densities of aptamers may render different kinetics and thermodynamics of aptamers binding of the targets. For instance, on-chip DNA hybridization efficiency is significantly influenced by the probe strand density. Different PDMS–AuNPs composite film immobilized with aptamers of different surface densities were independently prepared; it was achieved by allowing self-assembly in deposition solutions with a range of aptamer concentrations (0.1–5.0 μM). Darkness density decreased as the concentration of the covering aptamer solution was from 0.1 to 2.0 μM. As the concentration of aptamer ranges was from 2.0 to 5.0 μM, the darkness density gradually increased. The lower darkness density indicated the more compact of the film indirectly. As a result, 2.0 μM of aptamer was chosen to cover the composite film for the fabrication of aptamer-based sensor.

3.3. Silver enhancement time

Quantitative measurement of targets relies on the different darkness density of the microarrays, which related to silver enhancement process directly. To understand the system, a silver enhancement time optimization was performed. In our detection, color differences appeared during the process of silver reduction, and the same heavy darkness density appeared at the end of the reaction because of sliver reduction sufficiently. According to this phenomenon, data were collected at intervals during the whole reaction process. As time went on, more silver metal precipitated on the surface which made the color turn darker, and the slope of the calibration line reached the highest at the time of 30 min (see Fig. 4a). According to the above study, 30 min was chosen as the assay time in a compromise between the speed and the sensitivity of the sensor. The result in Fig. 4b indicated the darkness density increased along with silver enhancement time. The target of lysozyme concentration for each well is from 10^{-3} to 10^{3} μg/mL. Based on coactions between catalysis of AuNPs and catalysis inhibition of aptamer-target conjugations, the highest sensitivity, dependent on darkness density difference, is achieved at a certain time. After that point, silver enhancement reaction will be gradually completed which makes all the wells become the same darkness density finally (after 40 min).

3.4. Detection of biomolecules

At first, lysozyme was tested, the relationship between the concentration of lysozyme and the darkness density value was established, we took real time photos using ordinary digital camera at 30 min of silver enhancement. After analysing the live photos by image software, we could get obvious results as shown in Fig. 5. The darkness density value in the presence of lysozyme was higher than that in the absence of lysozyme, and it increased gradually with the increasing concentration of lysozyme from 10^{-4} to 1 μg/mL. The

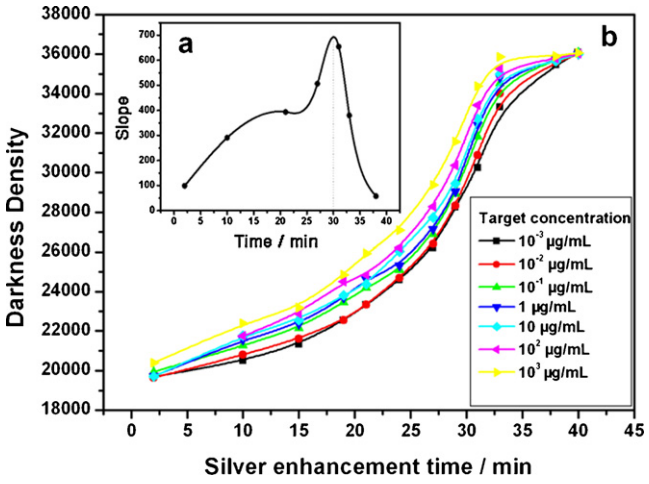

Fig. 4. Darkness density related to silver enhancement time for lysozyme with different concentrations (a) and the difference between darkness density (slope) versus silver enhancement time (b). Experimental conditions: 15 μL of silver enhancement solution was dropped into each well, the chip was incubated in dark and data were collected at intervals.

plot in Fig. 5a shows that the darkness density level is related to the logarithm of the lysozyme concentrations in a range from 10^{-4} to 1 μg/mL. Besides, the darkness density value is also linear to the lysozyme concentrations in a range from 10^{-1} to 1 μg/mL as shown in Fig. 5b.

The small biomolecules such as ATP were also tested. ATP has been introduced to the system as a special target molecule represented a series of small molecules. According to the study for ATP, anti-ATP aptamers could wrap ATP molecules around to form a three-way-junction structure (Lin and Patel, 1997). The binding event destroyed the strong inhibition ability of 'thick aptamer-MCH barrier layer' in various degree, then inhibiting ability decreased corresponding to the amount of ATP in the solution, and it directly lead to darkness density values differences in live photos. As shown in Fig. 6, quantitative behavior of aptamer-based assay was assessed with concentrations of ATP under the optimized conditions. The wide linear range for ATP detection spanning seven-order of magnitude was determined to be 1×10^{-4}–1×10^{3} μg/mL.

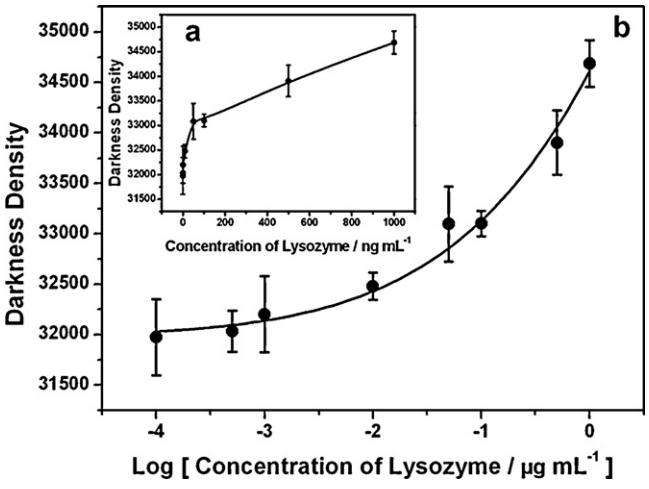

Fig. 5. Relationship between darkness density and concentration of lysozyme (a) darkness density related to logarithm of lysozyme concentration (b). Experimental conditions: 15 μL of lysozyme with different concentrations were dropped in the wells for 1 h at 37 °C. After rinsing process, 15 μL of silver enhancement solution was dropped into each well, the chip was incubated in dark for 30 min, live photos were captured with digital camera. The error bars represent average standard errors for three measurements.

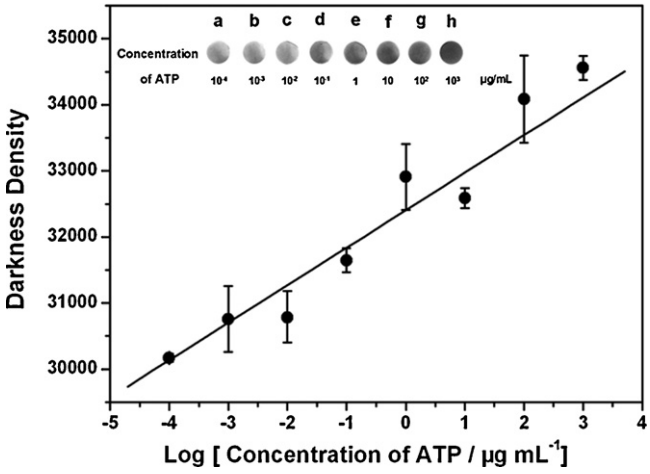

Fig. 6. Relationship between darkness density and logarithm of ATP concentration. The inset shows the photos of darkness density in wells. Experimental conditions were the same as those described in Fig. 5. The error bars represent average standard errors for three measurements.

4. Conslusions

A PDMS–AuNPs composite film-based aptamer sensor was developed. Coupled with silver enhancement colorimetric technique the detection time for protein and small biomolecules was less than 30 min, the determination limit is low to 1×10^{-4} μg/mL for both lysozyme and ATP. Moreover, this composite film is low-cost, convenient to carry with, as well as its ease of fabrication and operation. This device coupled with a digital camera eliminates the need for expensive, highly specialized equipment in diagnostic procedure. As a result, this device has great potential of developing into much more commercialized disposable test paper in the coming periods.

Acknowledgements

This work was supported by the National Natural Science Foundation of China (20821063, 20875080), National 863 program of China (2007AA022001), China Postdoctoral Science Foundation (200801372, 20070420982).

Appendix A. Supplementary data

Supplementary data associated with this article can be found, in the online version, at doi:10.1016/j.bios.2010.10.034.

References

Bai, X., Shao, C., Han, X., Li, Y., Guan, Y., Deng, Z., 2010. Biosens. Bioelectron. 25, 1984–1988.
Bercovici, M., Kaigala, G.V., Backhouse, C.J., Santiago, J.G., 2010. Anal. Chem. 82, 1858–1866.
Cai, H., Wang, Y., He, P., Fang, Y., 2002. Anal. Chim. Acta 469, 165–172.
Carvalhal, R.F., Kfouri, M.S., Piazetta, M.H.O., Gobbi, A.L., Kubota, L.T., 2010. Anal. Chem. 82, 1162–1165.
Chen, Z.P., Peng, Z.F., Luo, Y., Qu, B., Jiang, J.H., Zhang, X.B., Shen, G.L., Yu, R.Q., 2007. Biosens. Bioelectron. 23, 485–491.
Chen, S.J., Huang, Y.F., Huang, C.C., Lee, K.H., Lin, Z.H., Chang, H.T., 2008a. Biosens. Bioelectron. 23, 1749–1753.
Chen, Z., Li, G., Zhang, L., Jiang, J., Li, Z., Peng, Z., Deng, L., 2008b. Anal. Bioanal. Chem. 392, 1185–1188.
Cheng, A.K.H., Ge, B.X., Yu, H.Z., 2007. Anal. Chem. 79, 5158–5164.
Cherevko, S., Chung, C.H., 2009. Sens. Actuators, B 142, 216–223.
Gupta, S., Huda, S., Kilpatrick, P.K., Velev, O.D., 2007. Anal. Chem. 79, 3810–3820.
Hacker, G.W., 1989. In: Hayat, M.A. (Ed.), Methods And Applications, vol. 1. Academic Press, San Diego, CA, ch. 10.
Huang, Y.F., Chang, H.T., 2007. Anal. Chem. 79, 4852–4859.
Huang, C.C., Huang, Y.F., Cao, Z., Tan, W., Chang, H.T., 2005. Anal. Chem. 77, 5735–5741.
Jayasena, S.D., 1999. Clin. Chem. 45, 1628–1650.
Lin, C.H., Patel, D.J., 1997. Chem. Biol. 4, 817–832.
Liu, J., Lu, Y., 2006. Angew. Chem. Int. Ed. 45, 90–94.
Liu, J., Lu, Y., 2007. J. Am. Chem. Soc. 129, 8634–8643.
Liu, J.W., Mazumdar, D., Lu, Y., 2006. Angew. Chem. Int. Ed. 45, 7955–7959.
Lutz, S., Weber, P., Focke, M., Faltin, B., Hoffmann, J., Muller, C., Mark, D., Roth, G., Munday, P., Armes, N., Piepenburg, O., Zengerle, R., Stetten, F.V., 2010. Lab Chip 10, 887–893.
Martinez, A.W., Philips, S.T., Carrilho, E., Thomas, S.W., Sindi, H., Whitesides, G.M., 2008. Anal. Chem. 80, 3699–3707.
Miao, F.J., Tao, B.R., Sun, L., Liu, T., You, J.C., Wang, L.W., Chu, P.K., 2009. Sens. Actuators, B 141, 338–342.
Nogami, M., Maeda, T., Uma, T., 2009. Sens. Actuators, B 137, 603–607.
Pan, Q., Zhang, R.Y., Bai, Y.F., Hen, N.Y., Lu, Z.H., 2008. Anal. Biochem. 375, 179–186.
Rodriguez, M.C., Kawde, A.N., Wang, J., 2005. Chem. Commun., 4267–4269.
Ronen, C.H., Borzin, E., Gerchikov, Y., Tessler, N., Eichen, Y., 2009. Chem. Eur. J. 15, 10380–10386.
Sia, S.K., Kricka, L.J., 2008. Lab Chip 8, 1982–1983.
Song, Y., Zhao, C., Ren, J., Qu, X., 2009. Chem. Commun., 1975–1977.
Wang, B., Chen, K., Jiang, S., Reincke, F., Tong, W.J., Wang, D.Y., Gao, C.Y., 2006. Biomacromolecules 7, 1203–1209.
Wang, J., Wang, L., Liu, X., Liang, Z., Song, S., Li, W., Li, G., Fan, C., 2007. Adv. Mater. 19, 3943–3946.
Wang, J., Munir, A., Li, Z., Zhou, H.S., 2009. Biosens. Bioelectron. 25, 124–129.
Wilson, D.S., Szostak, J.W., 1999. Annu. Rev. Biochem. 68, 611–647.
Wu, W.Y., Bian, Z.P., Wang, W., Wang, W., Zhu, J.J., 2010. Sens. Actuators, B 147, 298–303.
Xu, L.J., Du, J.J., He, N.Y., Deng, Y., Li, S., Wang, T., 2009. J. Nanosci. Nanotechnol. 9, 2698–2703.
Yang, M.H., Wang, C.C., 2009. Anal. Biochem. 385, 128–131.
Yang, M.H., Sun, S., Kostov, Y., Rasooly, A., 2010. Lab Chip 10, 1011–1017.
Yeh, C.H., Huang, H.H., Chang, T.C., Lin, H.P., Lin, Y.C., 2009. Biosens. Bioelectron. 24, 1661–1666.
Zhang, Q., Xu, J.J., Liu, Y., Chen, H.Y., 2008. Lab Chip 8, 352–357.
Zhang, Z., Chen, C.L., Zhao, X.S., 2009. Electroanalysis 21, 1316–1320.